



SOCIETY FOR APPLIED MICROWAVE ELECTRONICS ENGINEERING AND RESEARCH

R&D Laboratory under Ministry of Electronics and Information
Technology (MeitY)

Internship Report

Animesh Kumar

July 23, 2025

Internship Report

Surface Coil Sensitivity Correction and SENSE Reconstruction in MRI

Submitted by

Animesh Kumar

Department of Electrical Engineering

IIT Bombay

Internship Organization:

**SOCIETY FOR APPLIED MICROWAVE
ELECTRONICS ENGINEERING AND
RESEARCH (SAMEER)**

R&D Laboratory under Ministry of Electronics and Information
Technology (MeitY)

Supervisor:

Divakara Annappa

July 23, 2025

Acknowledgements

I would like to express my sincere gratitude to **Mr. Divakara Annappa**, my internship supervisor at SAMEER, for his invaluable guidance, support, and encouragement throughout the course of this project. His mentorship and thoughtful insights played a vital role in shaping this work.

I am also deeply thankful to **Professor Vikram Gadre**, my faculty advisor at IIT Bombay, for his academic guidance, continuous motivation, and for providing me with the opportunity to undertake this internship. His perspective and feedback greatly contributed to the development of this project.

Contents

Acknowledgements	1
Contents	2
1 Introduction	4
2 Background and Literature Review	5
2.1 Introduction to Intensity Non-Uniformity in MRI	5
2.2 Mathematical Model of Intensity Non-Uniformity	5
2.3 Prospective vs Retrospective Correction Methods	6
2.3.1 Prospective Methods	6
2.3.2 Retrospective Correction Methods	6
2.4 Surface Coil Sensitivity and its Correction	6
2.5 Intensity Non-Uniformity in MRI	7
2.6 Wavelet-Based Bias Field Estimation	7
2.7 Parallel Imaging and SENSE	8
2.8 Relevance and Integration	8
2.9 Summary	8
3 Methodology	9
3.1 Wavelet Based Approximation with Iterative MVP	9
3.1.1 Mathematical Model of Bias Field	9
3.1.2 Wavelet-Based Multi-Resolution Analysis (MRA)	9
3.1.3 Initial Sensitivity Profile Estimation	10
3.1.4 Iterative Maximum Value Projection (MVP)	11
3.1.5 Bias Field Correction	11
3.1.6 Inhomogeneity Index and Optimal Scale Selection	11
3.1.7 Experimental Setup and Tools	12
3.1.8 Results	13
3.2 Wavelet Based Approximation + Iterative MVP using FSL BET for extracting Brain	14
3.2.1 Results	14

3.3	Energy-Based Thresholding with Iterative MVP	15
3.3.1	Results	16
3.4	Extrapolation-Based Bias Field Estimation	18
3.4.1	Results: Extrapolation Method	19
4	Reconstruction Process	21
4.1	Aim	21
4.2	Methodology	21
4.2.1	Simulating Coil Sensitivity Profiles	21
4.2.2	Simulating Undersampled Aliased Data	21
4.2.3	Bias Field Estimation using MVP	22
4.2.4	SENSE-like Reconstruction	22
4.3	Results and Observations	23
4.4	Bias Field Correction Results	23
4.4.1	Coil-wise Results	23
4.4.2	Tikhonov-Regularized SENSE Reconstruction	25
5	Conclusion and Future Work	26
5.1	Conclusion	26
5.2	Future Work	26

1. Introduction

Magnetic Resonance Imaging (MRI) is an indispensable tool in medical diagnostics, offering unparalleled soft tissue contrast and spatial resolution without ionizing radiation. However, the quality and quantitative accuracy of MRI scans are often compromised by intensity non-uniformities, particularly when surface coils are used for signal acquisition. These inhomogeneities arise from the spatially varying sensitivity profiles of the surface coils, resulting in images with spatially inconsistent brightness. This intensity bias not only affects visual interpretation but also degrades the performance of downstream image processing tasks such as segmentation, registration, and quantitative analysis.

Several methods have been developed over the years to correct for such non-uniformities. One classic approach is the use of fuzzy segmentation algorithms, which leverage intensity clustering and spatial constraints to iteratively estimate and correct the bias field. These techniques, while effective, are sensitive to noise and the accuracy of initial assumptions.

In contrast, wavelet-based methods provide a more mathematically grounded and multiscale approach to bias estimation. Lin et al. introduced the Maximum Value Projection (MVP) method using biorthogonal wavelets to decompose an MRI slice into low-frequency (bias) and high-frequency (anatomical detail) components. The algorithm iteratively enhances the low-frequency approximation while suppressing detail coefficients, thus isolating the bias field in a spatially smooth and data-driven manner .

Simultaneously, the advent of parallel imaging techniques like SENSE (Sensitivity Encoding) has addressed the challenge of long acquisition times in MRI. By undersampling k-space and using spatial encoding provided by multiple surface coils, SENSE reconstructs full-FOV images from aliased data. A critical prerequisite for SENSE is the availability of accurate coil sensitivity maps, which are typically estimated from separate calibration scans or autocalibration data. However, the assumption of known and smooth coil sensitivities is often violated in practice.

The primary objective of this internship project was to develop a wavelet-based Maximum-Value-Projection (MVP) bias correction method and integrate it into a SENSE-like MRI reconstruction pipeline to enhance image quality and reduce residual artifacts. This project lies at the intersection of image processing, mathematical modeling, and signal reconstruction—demonstrating how a careful estimation of bias fields can significantly improve the performance of accelerated MRI reconstruction techniques.

2. Background and Literature Review

2.1. Introduction to Intensity Non-Uniformity in MRI

Magnetic Resonance Imaging (MRI) is widely utilized in clinical and research environments due to its non-invasive nature and superior soft tissue contrast. However, the quality of MR images is frequently compromised by various artifacts. One such artifact is **intensity non-uniformity (INU)**, also known as *bias field*, a spatially slow-varying, multiplicative field that distorts the true image intensities across the field of view.

This artifact may arise from several sources including B_0 inhomogeneities, coil sensitivity variations (especially with surface coils), and dielectric resonance effects. The resultant images exhibit unrealistic smooth gradients in intensity which can severely affect subsequent automated tasks like segmentation and registration.

2.2. Mathematical Model of Intensity Non-Uniformity

A widely adopted model to represent INU-contaminated MRI data is the **multiplicative model with additive noise**, given by:

$$v(\mathbf{r}) = g(\mathbf{r}) \cdot u(\mathbf{r}) + n(\mathbf{r}) \quad (2.1)$$

where:

- $v(\mathbf{r})$ is the observed intensity at spatial position $\mathbf{r} = (x, y, z)$,
- $u(\mathbf{r})$ is the true, bias-free intensity,
- $g(\mathbf{r})$ is the smooth gain field or bias field,
- $n(\mathbf{r})$ represents Rician-distributed noise.

The goal of INU correction is to estimate $u(\mathbf{r})$ from $v(\mathbf{r})$, which is ill-posed since both g and u are unknown. This necessitates assumptions or constraints, such as smoothness of $g(\mathbf{r})$ and piecewise constancy of $u(\mathbf{r})$.

2.3. Prospective vs Retrospective Correction Methods

2.3.1 Prospective Methods

These techniques aim to mitigate INU during acquisition. For instance:

- Using body coils instead of surface coils to ensure uniform B1 field.
- Acquiring images of uniform phantoms to calibrate coil sensitivity.
- Active RF modulation using LUTs (Clare et al., 2001) or customized excitation pulses (Deichmann et al., 2002).

While effective, these methods require hardware modification or longer scan times and are not feasible in many clinical settings.

2.3.2 Retrospective Correction Methods

These techniques operate purely on the acquired data and are more practical. They are classified based on assumptions made about the bias field or image content:

1. **Surface Fitting Methods:** Approximate $g(\mathbf{r})$ with smooth functions like splines or polynomials (e.g., Legendre).
2. **Spatial Filtering Methods:** Use low-pass or homomorphic filters to isolate and divide out low-frequency bias components.
3. **Statistical Methods:** Model the image as a finite Gaussian mixture and apply EM algorithms for bias estimation, incorporating spatial priors via Markov Random Fields (Wells et al., 1996; Van Leemput et al., 1999).
4. **Wavelet-Based Methods:** Use discrete wavelet transform (DWT) to isolate the low-frequency bias in approximation subbands and suppress it (Han et al., 2001).

2.4. Surface Coil Sensitivity and its Correction

Surface coils enhance signal-to-noise ratio (SNR) locally but introduce strong bias fields due to their inhomogeneous sensitivity profiles. A key strategy for their correction is sensitivity profiling followed by voxel-wise division.

Let $S_i(\mathbf{r})$ denote the sensitivity of the i -th coil, then the image from that coil is:

$$v_i(\mathbf{r}) = S_i(\mathbf{r}) \cdot u(\mathbf{r}) + n_i(\mathbf{r}) \quad (2.2)$$

Wavelet-based estimation treats $S_i(\mathbf{r})$ as a low-frequency surface. It leverages DWT to isolate the approximation coefficients and model sensitivity. After estimating S_i , the bias-free image is obtained as:

$$u(\mathbf{r}) = \frac{v_i(\mathbf{r})}{\hat{S}_i(\mathbf{r})} \quad (2.3)$$

where \hat{S}_i is the estimated sensitivity profile.

2.5. Intensity Non-Uniformity in MRI

MRI images acquired with surface coils often suffer from **intensity non-uniformity (INU)** due to spatial variations in coil sensitivity. This bias appears as a low-frequency multiplicative field:

$$I_{\text{measured}}(x, y) = B(x, y) \cdot I_{\text{true}}(x, y), \quad (2.4)$$

where $B(x, y)$ is the bias field, and I_{true} is the ideal image.

Traditional methods like fuzzy segmentation (Belaroussi et al. [?]) model MR images as mixtures of tissue classes and iteratively estimate $B(x, y)$ by minimizing an energy function:

$$J(U, B) = \sum_{i=1}^N \sum_{j=1}^C u_{ij}^m \|I_i - B_i c_j\|^2 + \lambda \cdot \text{Reg}(U), \quad (2.5)$$

where u_{ij} is the fuzzy membership, c_j class mean, and $\text{Reg}(U)$ enforces spatial smoothness.

However, these segmentation-based methods suffer from sensitivity to noise and rely heavily on accurate initialization and tissue homogeneity assumptions. As an alternative, a wavelet-based method leverages the multiscale decomposition of MRI images using biorthogonal wavelets to isolate the bias field.

2.6. Wavelet-Based Bias Field Estimation

Lin et al. introduced a wavelet-based method using biorthogonal decomposition to extract the bias field from MR images. In the MVP (Maximum-Value Projection) algorithm, the image is decomposed into approximation coefficients A_j and detail coefficients (H_j, V_j, D_j) at level j . The bias field is assumed to reside in the smooth approximation:

$$I = A_j + H_j + V_j + D_j. \quad (2.6)$$

To extract a smooth bias field estimate, the algorithm suppresses the high-frequency detail coefficients and iteratively reconstructs the approximation, retaining only the large-scale intensity trends. The final bias field is computed by back-projecting the modified wavelet coefficients and applying exponential smoothing in log space to preserve multiplicativity.

The MVP method showed robustness to anatomical variation and intensity heterogeneity, especially in phantom and real datasets. Compared to fuzzy and polynomial models, the wavelet-based technique requires fewer assumptions and achieves visually smooth corrections.

2.7. Parallel Imaging and SENSE

To reduce MRI acquisition time, parallel imaging techniques like SENSE (Sensitivity Encoding) utilize multiple receiver coils with distinct spatial sensitivities. In SENSE, an undersampled k-space dataset is reconstructed by solving a system of linear equations at each pixel location, using the known sensitivity profiles of the coils. If the acceleration factor is R , then the acquired image is aliased R -fold, and the unfolding system can be written as:

$$\mathbf{y} = \mathbf{S} \cdot \boldsymbol{\rho}, \quad (2.7)$$

where $\mathbf{y} \in \mathbb{C}^C$ is the observed aliased signal from C coils, $\mathbf{S} \in \mathbb{C}^{C \times R}$ contains the coil sensitivities at each alias location, and $\boldsymbol{\rho} \in \mathbb{C}^R$ is the vector of true unaliased pixel values to be estimated.

The least-squares solution is obtained by computing the pseudoinverse:

$$\hat{\boldsymbol{\rho}} = (\mathbf{S}^H \mathbf{S})^{-1} \mathbf{S}^H \mathbf{y}. \quad (2.8)$$

However, the quality of reconstruction is heavily dependent on the accuracy and smoothness of the coil sensitivity maps. Errors in these maps lead to residual aliasing and noise amplification. The integration of wavelet-based MVP-estimated sensitivities into SENSE helps provide smooth and data-driven estimates, which improves the conditioning of the unfolding matrix $\mathbf{S}^H \mathbf{S}$ and stabilizes the reconstruction.

2.8. Relevance and Integration

Compared to B1-mapping or ESPIRiT-based estimation, the MVP approach offers simplicity, robustness, and compatibility with preprocessed or simulated datasets. This makes it ideal for research pipelines, particularly when raw calibration data is unavailable.

In this project, MVP-based bias correction is integrated with synthetic coil modeling and SENSE-like unfolding to form a complete MRI reconstruction pipeline.

2.9. Summary

The bias field correction remains a critical preprocessing step in quantitative MRI. Among various methods, wavelet-based and statistical approaches offer a good tradeoff between accuracy and practicality, especially when combined with segmentation and reconstruction pipelines such as SENSE.

3. Methodology

3.1. Wavelet Based Approximation with Iterative MVP

3.1.1 Mathematical Model of Bias Field

MRI images acquired using phased-array surface coils often suffer from intensity non-uniformity caused by spatially varying sensitivity profiles. This can be modeled as:

$$v(\mathbf{r}) = g(\mathbf{r}) \cdot u(\mathbf{r}) + n(\mathbf{r}), \quad (3.1)$$

where:

- $v(\mathbf{r})$ is the observed voxel intensity at location \mathbf{r} ,
- $g(\mathbf{r})$ is the multiplicative bias field (coil sensitivity profile),
- $u(\mathbf{r})$ is the true underlying anatomical image,
- $n(\mathbf{r})$ is additive noise, assumed to follow a Rician distribution.

The goal is to estimate $g(\mathbf{r})$ and reconstruct a bias-corrected image:

$$\hat{u}(\mathbf{r}) = \frac{v(\mathbf{r})}{\hat{g}(\mathbf{r}) + \epsilon}, \quad (3.2)$$

where $\hat{g}(\mathbf{r})$ is the estimated sensitivity profile and ϵ is a small constant added to avoid division by zero.

3.1.2 Wavelet-Based Multi-Resolution Analysis (MRA)

We apply a Discrete Wavelet Transform (DWT) using the biorthogonal Daubechies 9/7 (Daub97) filter to decompose the image into a hierarchy of frequency bands:

- **Low-pass (LL):** captures slowly varying intensity patterns, which represent the bias field.
- **High-pass (LH, HL, HH):** captures sharp anatomical features such as edges and tissue boundaries.

Mathematically, at decomposition level l , the observed image $v(\mathbf{r})$ can be expressed as:

$$v(\mathbf{r}) = A_l(\mathbf{r}) + \sum_{i=1}^l D_i(\mathbf{r}), \quad (3.3)$$

where $A_l(\mathbf{r})$ is the approximation (LL) component capturing low-frequency content, and $D_i(\mathbf{r})$ are the detail coefficients from level i capturing high-frequency anatomical information.

Why use Daub97? The Daubechies 9/7 wavelet (known as `bior4.4` in PyWavelets) is a linear phase biorthogonal filter, which helps to preserve spatial alignment (no pixel shifts) during analysis and reconstruction. This is crucial for medical imaging where geometric fidelity is important.

It is also widely used in image compression standards such as JPEG2000 due to its strong energy compaction, smoothness, and ability to preserve structural integrity - properties that make it well-suited for intensity correction in MRI.

Vanishing Moments of Daub97:

- The **analysis scaling function** ϕ has 4 vanishing moments, enabling it to ignore polynomials up to degree 3 in the approximation (low-pass) branch.
- The **synthesis wavelet function** ψ also has 4 vanishing moments, enabling accurate reconstruction of smooth regions from wavelet coefficients.

This ensures that slowly varying multiplicative bias fields, which are inherently low-frequency phenomena, are well modeled in the LL subbands across scales.

3.1.3 Initial Sensitivity Profile Estimation

Following wavelet-based decomposition, the approximation component at a given scale l captures low-frequency components of the image. Given that the coil sensitivity bias field $g(\mathbf{r})$ varies slowly across space, the low-pass subband (LL) at level l serves as a reasonable initial estimate of the bias field:

$$\hat{g}_l^{(0)}(\mathbf{r}) = A_l(\mathbf{r}), \quad (3.4)$$

where $A_l(\mathbf{r})$ denotes the approximation image at level l . However, due to the inherent nature of low-pass filtering, high-intensity anatomical boundaries, particularly near air-tissue interfaces, are smoothed out. This leads to an underestimation of the bias field in such regions. This underestimation must be compensated for to avoid overcorrection in the final bias-normalized image.

3.1.4 Iterative Maximum Value Projection (MVP)

To refine the initial estimate $\hat{g}_l^{(0)}$, an iterative correction strategy based on Maximum Value Projection (MVP) is employed. This iterative scheme mitigates the underestimation near strong edges by iteratively projecting the maximum pixel values between the current estimate and the original image:

1. At iteration k , compute the maximum value projection:

$$M_l^{(k)}(\mathbf{r}) = \max \left(v(\mathbf{r}), \hat{g}_l^{(k)}(\mathbf{r}) \right), \quad (3.5)$$

where $v(\mathbf{r})$ is the observed intensity at location \mathbf{r} .

2. Apply wavelet decomposition to $M_l^{(k)}$ and extract the new approximation component:

$$\hat{g}_l^{(k+1)}(\mathbf{r}) = A_l^{(k+1)}(\mathbf{r}). \quad (3.6)$$

3. Repeat steps (1) and (2) until convergence is reached:

$$\frac{\|\hat{g}_l^{(k+1)} - \hat{g}_l^{(k)}\|_2^2}{\|\hat{g}_l^{(k)}\|_2^2} < \delta, \quad (3.7)$$

where δ is a small threshold (typically $\delta = 0.01$) indicating stability in the estimate.

This process is repeated independently for multiple decomposition levels $l = 1, 2, \dots, L$. Each level yields a distinct estimate of the sensitivity profile \hat{g}_l , which is then used for intensity normalization.

3.1.5 Bias Field Correction

Once the refined estimate $\hat{g}_l(\mathbf{r})$ is obtained at each scale l , the bias corrected image is calculated by voxel-wise division of the original image by the estimated sensitivity profile:

$$\hat{u}_l(\mathbf{r}) = \frac{v(\mathbf{r})}{\hat{g}_l(\mathbf{r}) + \epsilon}, \quad (3.8)$$

where ϵ is a small regularization constant (e.g., $\epsilon = 10^{-5}$) added to avoid numerical instability in low-signal regions.

3.1.6 Inhomogeneity Index and Optimal Scale Selection

Choosing the appropriate level of decomposition l is critical as lower levels may retain residual anatomical information in \hat{g}_l , while higher levels may oversmooth the true bias field. To automate this selection, an inhomogeneity index I_l is defined for each level:

$$I_l = \frac{V_l}{C_l \cdot \sigma_l}, \quad (3.9)$$

where:

- V_l : intra-tissue variance in $\hat{u}_l(\mathbf{r})$: low values are preferred,
- C_l : inter-tissue contrast in $\hat{u}_l(\mathbf{r})$: higher is better,
- σ_l : spatial smoothness of the estimated bias field $\hat{g}_l(\mathbf{r})$: higher smoothness indicates a physically plausible sensitivity map.

These quantities are estimated as follows:

- **Tissue modeling**: Gaussian Mixture Modeling (GMM) is applied to the histogram of $\hat{u}_l(\mathbf{r})$ to segment tissues into classes (e.g., gray matter, white matter, fat).
- **Intra-tissue variance** V_l is computed as the sum of variances within each GMM cluster.
- **Inter-tissue contrast** C_l is computed as the difference between maximum and minimum cluster means.
- **Smoothness** σ_l is measured via spatial total variation or discrete gradient norm of \hat{g}_l .

The optimal level l^* is selected as:

$$l^* = \arg \min_l I_l. \quad (3.10)$$

The corrected image $\hat{u}_{l^*}(\mathbf{r})$ corresponding to the minimal inhomogeneity index is selected as the final output.

3.1.7 Experimental Setup and Tools

- Dataset: BrainWeb simulated T1 or T2-weighted images with 20% intensity inhomogeneity.
- Tools: Python, pywt for wavelet transforms, FSL-BET for brain masking.
- Parameters: Daub97 wavelets, decomposition up to 10 levels, MVP convergence threshold $\delta = 0.01$.

3.1.8 Results

Table 3.1: Convergence statistics and inhomogeneity index across wavelet decomposition levels.

Level	Iterations to Converge	Inhomogeneity Index
1	56	155.5128
2	48	126.1230
3	37	27.2569
4	50	30.2664
5	44	13.1983
6	22	31.5379
7	12	63.3482

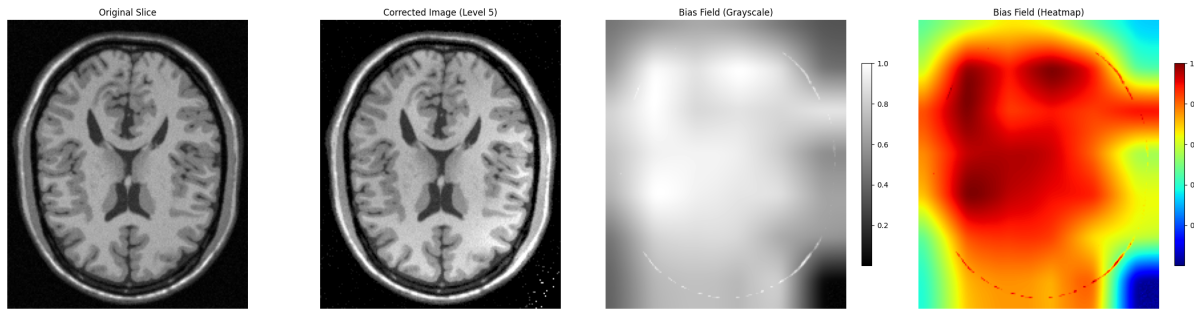


Figure 3.1: Visualization of wavelet-based bias field correction using MVP at Level 5. From left to right: (1) Original T1-weighted MRI slice with simulated intensity inhomogeneity (20%), (2) Corrected image after bias field normalization using estimated sensitivity profile, (3) Estimated bias field shown in grayscale, highlighting smooth intensity drift across the brain, (4) Bias field shown as a heatmap, where warmer colors indicate higher sensitivity and cooler colors reflect attenuation.

Inference

The appearance of a bright white ring in the estimated bias field near the brain boundary suggests that the algorithm assigns high coil sensitivity in this region. However, this area lies close to the air-tissue interface, where the MRI signal typically decreases. The elevated intensity is likely due to anatomical edge contrast rather than actual coil behavior. This leads to overestimation of the bias field outside the brain, reinforcing the importance of incorporating brain masking (e.g., using FSL-BET) to constrain bias estimation within anatomically valid regions.

3.2. Wavelet Based Approximation + Iterative MVP using FSL BET for extracting Brain

This method combines wavelet-based multi-resolution analysis with iterative Maximum Value Projection (MVP) to estimate the bias field in MRI. A biorthogonal wavelet (Daub97) is used to isolate low-frequency components that approximate the slowly varying coil sensitivity profile. To prevent bias estimation in non-anatomical regions, brain masking is performed using FSL’s Brain Extraction Tool (BET). This restricts the MVP iterations to within the brain region, reducing artifacts from edge contrast near air–tissue boundaries and improving the accuracy of the final bias-corrected image.

3.2.1 Results

Table 3.2: Convergence statistics and inhomogeneity index across wavelet decomposition levels using FSL-BET masking.

Level	Iterations to Converge	Inhomogeneity Index
1	44	24.1922
2	48	19.6806
3	15	32.2367
4	63	9.1081
5	33	28.0013
6	22	33.8063
7	23	44.7159

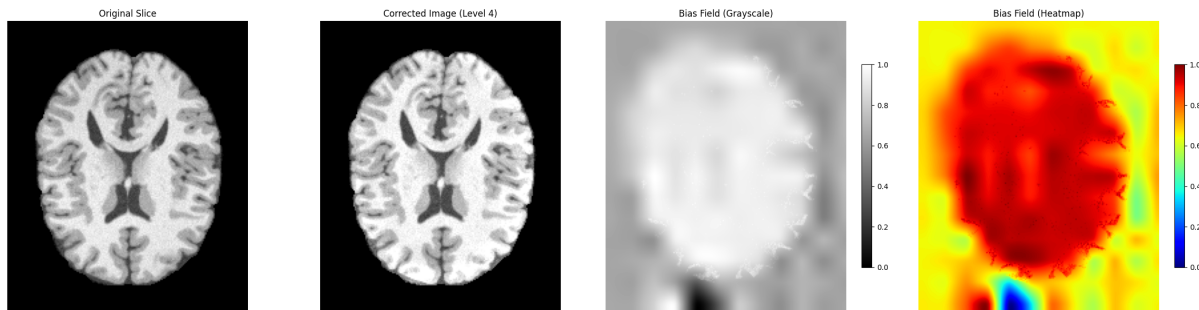


Figure 3.2: Visualization of wavelet-based bias field correction using MVP at Level 4 using FSL-BET masking. From left to right: (1) Original T1-weighted MRI slice with simulated intensity inhomogeneity (20%), (2) Corrected image after bias field normalization using estimated sensitivity profile, (3) Estimated bias field shown in grayscale, highlighting smooth intensity drift across the brain, (4) Bias field shown as a heatmap, where warmer colors indicate higher sensitivity and cooler colors reflect attenuation.

Inference

The use of FSL-BET for anatomical masking improves the bias field estimation by limiting the analysis to brain tissue and excluding non-anatomical regions. This results in a lower

optimal inhomogeneity index (9.1081 at Level 4), compared to the previous case without masking (13.1983 at Level 5), indicating a more accurate and spatially smooth correction.

However, despite this improvement, some anatomical features are still visible in the estimated bias field, particularly near the brain boundary. This suggests that residual edge artifacts persist, likely due to the proximity of high-contrast anatomical structures. Furthermore, the boundary extracted by FSL-BET may not perfectly align with the true anatomical contour, which complicates the wavelet-based filtering and leads to under-smoothing near the edges. Consequently, the bias field remains complex in boundary regions, though overall performance is enhanced by masking.

3.3. Energy-Based Thresholding with Iterative MVP

This method aims to estimate and correct intensity non-uniformity (bias field) in MRI using wavelet-based decomposition combined with iterative Maximum-Value Projection (MVP) and energy thresholding.

The core idea is to isolate the low-frequency bias field by suppressing high-frequency anatomical structures through controlled wavelet reconstruction. At a given decomposition level, the algorithm proceeds as follows:

1. The input image is decomposed using the Discrete Wavelet Transform (DWT).
2. All detail coefficients (i.e., LH, HL, HH) representing high-frequency content are set to zero.
3. The image is reconstructed using only the approximation coefficients (LL), with the low-frequency content retained.
4. This reconstructed image, which serves as an estimate of the bias field, is combined with the original image via element-wise Maximum-Value Projection (MVP) to preserve anatomical structure.
5. The detail energy of the current iteration is computed and compared with the initial detail energy:

$$\text{Energy Ratio} = \frac{E_{\text{detail}}^{(k)}}{E_{\text{detail}}^{(0)}}. \quad (3.11)$$

The iteration continues until the energy ratio falls below a user-defined threshold (e.g., 0.05), ensuring that the residual high-frequency content is sufficiently suppressed.

This process is repeated independently on multiple decomposition levels. For each level l , a bias corrected image \hat{u}_l is generated and evaluated using an inhomogeneity index I_l that accounts for both intra-tissue variance and spatial smoothness of the estimated bias field.

The optimal decomposition level l^* is selected as:

$$l^* = \arg \min_l I_l, \quad (3.12)$$

balancing the trade-off between effective bias field smoothing and preservation of anatomical details.

3.3.1 Results

Table 3.3: Convergence statistics, inhomogeneity index, and energy ratio across wavelet decomposition levels using energy-based MVP with KMeans masking.

Level	Iterations	Inhomogeneity Index	Energy Ratio (%)
1	50	78.2704	25.93
2	50	160.6639	53.44
3	16	27.7104	5.79
4	3	22.7749	11.56
5	2	18.5722	21.14
6	2	26.4867	28.63
7	3	55.3380	77.15
8	1	185.4709	100.00
9	1	185.4709	100.00
10	1	185.4709	100.00

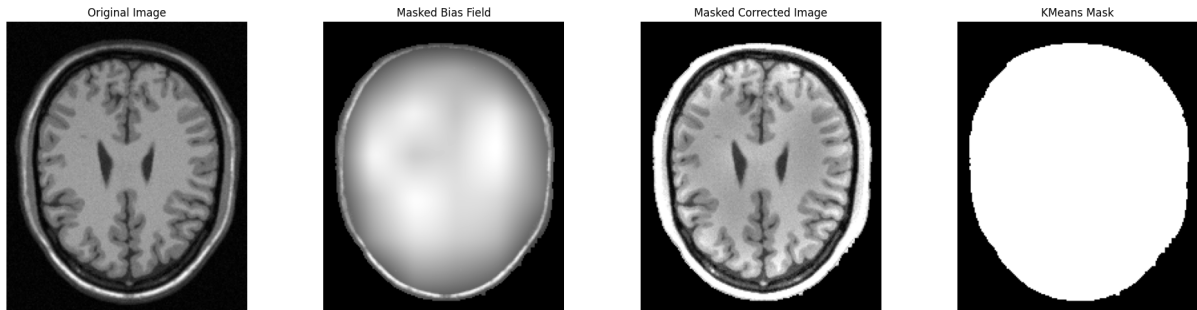


Figure 3.3: Visualization of the bias field correction pipeline using energy-based MVP with KMeans masking. From left to right: (1) Original T1-weighted MRI slice with intensity inhomogeneity, (2) Estimated low-frequency bias field constrained within the anatomical region via KMeans-derived mask, (3) Corrected image after bias field division and masking, showing improved tissue contrast, (4) Binary brain mask generated using KMeans clustering to separate foreground from background on the original slice.

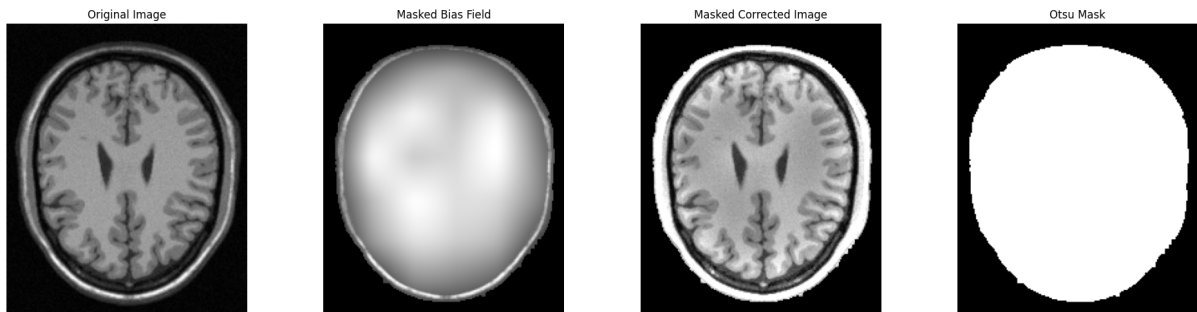
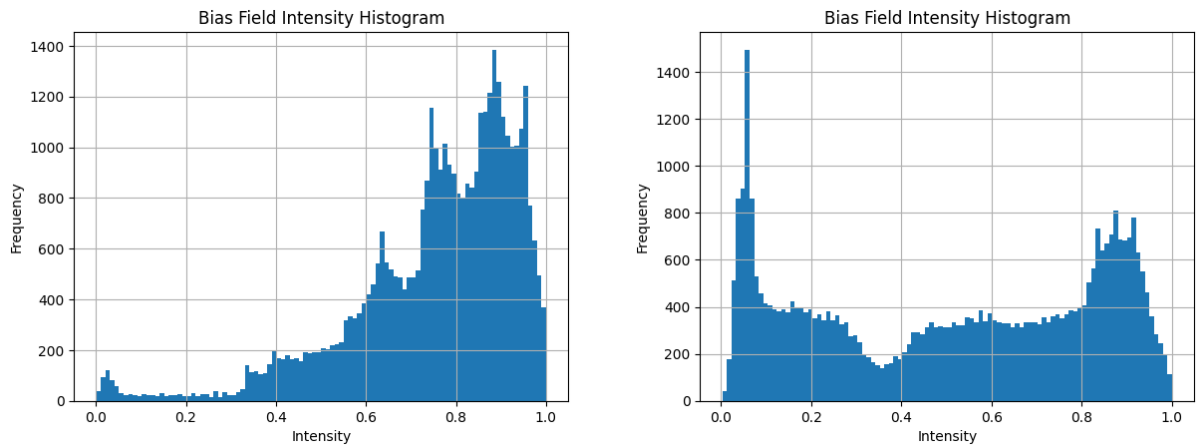


Figure 3.4: Bias field correction pipeline using Otsu thresholding for anatomical masking. From left to right: (1) Original MRI slice with intensity non-uniformity, (2) Estimated low-frequency bias field constrained by Otsu-based brain mask, (3) Bias-corrected image showing improved homogeneity, (4) Binary mask generated via Otsu thresholding for foreground-background separation on the original slice.



(a) Bias Field intensity histogram od Method 1 : Wavelet Based Approximation with Iterative MVP

(b) Bias Filed intensity histogram od Method 3 : Energy-Based Thresholding with Iterative MVP

Figure 3.5: Comparison of bias field intensity histograms for two correction methods. **Left:** Wavelet-Based Approximation with Iterative MVP shows multiple sharp peaks, indicating that anatomical structures have not been fully removed from the bias field estimate and insufficient smoothing of the bias field.

Right: Energy-Based Thresholding with Iterative MVP produces a smoother, more compact histogram with reduced variation and fewer peaks. The isolated peak near zero arises due to background voxels retained after masking via Kmeans/Otsu, while the tissue-related bias values are tightly concentrated, suggesting better bias separation and smoothness.

3.4. Extrapolation-Based Bias Field Estimation

This method is designed to correct intensity inhomogeneity (bias field) in MRI by extrapolating image intensities beyond the anatomical region using nearest-neighbor projection, followed by multi-resolution wavelet smoothing. The process consists of the following steps:

1. Anatomical Boundary Detection: We begin by identifying the anatomical region through intensity thresholding and morphological operations. Given a 2D MRI slice $v(\mathbf{r})$, we compute a binary mask $M(\mathbf{r}) \in \{0, 1\}$ where 1 denotes tissue. Noise is removed by thresholding the lower percentile intensities. Holes are filled, and the structure is refined using binary erosion and dilation. The boundary ∂M is extracted via:

$$\partial M = M - \text{erode}(M). \quad (3.13)$$

2. Image Extrapolation via Nearest Neighbor Projection: To allow wavelet filtering to operate seamlessly near the edges, the image is extrapolated beyond the anatomical region. For every background pixel $\mathbf{r} \notin M$, we locate its nearest neighbor $\mathbf{r}' \in M$ using a Euclidean distance transform and assign:

$$v_{\text{ext}}(\mathbf{r}) = v(\mathbf{r}'), \quad \text{where } \mathbf{r}' = \arg \min_{\mathbf{q} \in M} \|\mathbf{r} - \mathbf{q}\|_2. \quad (3.14)$$

This results in a smooth extension of the image where background pixels adopt values of their nearest anatomical neighbors, avoiding boundary artifacts and preserving continuity.

3. Multi-Resolution Wavelet Smoothing: The extrapolated image $v_{\text{ext}}(\mathbf{r})$ is decomposed using a discrete wavelet transform (DWT) with Daubechies-16 (db16) filters up to level L :

$$v_{\text{ext}}(\mathbf{r}) \xrightarrow{\text{DWT}} \{A_L, D_1, \dots, D_L\}, \quad (3.15)$$

where A_L is the approximation at level L , and D_i are the detail coefficients. All D_i are zeroed out, retaining only A_L . The smoothed bias field $\hat{g}_L(\mathbf{r})$ is reconstructed by inverse wavelet transform:

$$\hat{g}_L(\mathbf{r}) = \text{IDWT}(A_L, 0, \dots, 0). \quad (3.16)$$

4. Bias Field Correction and Entropy-Based Optimization: The corrected image is computed as:

$$\hat{u}_L(\mathbf{r}) = \frac{v(\mathbf{r})}{\hat{g}_L(\mathbf{r}) + \epsilon}, \quad (3.17)$$

where ϵ is a small constant to avoid division by zero. Among all levels $L = 1, \dots, 7$, the optimal level is chosen by minimizing Shannon entropy of the corrected image:

$$H(\hat{u}_L) = - \sum_i p_i \log_2 p_i, \quad (3.18)$$

where p_i is the normalized histogram of intensity values. Lower entropy corresponds to a more uniform, bias-corrected image.

Motivation for Extrapolation: Without extrapolation, wavelet filters applied near the edge of the anatomy suffer from boundary artifacts, causing intensity distortions and ringing. By extending the image using nearest-neighbor values from within the anatomy, we provide a natural continuation that improves the performance of the wavelet-based smoothing. This is especially crucial when high-order wavelets like Daubechies-16 are used, which have long filter lengths and are sensitive to boundary conditions.

3.4.1 Results: Extrapolation Method

The extrapolation method was applied using nearest-neighbor boundary extension and wavelet-based multi-resolution smoothing (db16). Entropy was used as the optimization criterion, with the lowest entropy indicating the best bias correction. The results across levels are shown below:

Table 3.4: Entropy values at each decomposition level for nearest-neighbor extrapolation method.

Level	Entropy
1	0.0624
2	0.1703
3	0.6541
4	0.4794
5	0.0284
6	0.0691
7	6.9786

The optimal decomposition level was found to be **level 5**, which yielded the minimum Shannon entropy of **0.0284**, indicating the image most homogeneously corrected for bias.

Alternative Approach — Mirror Extrapolation: Instead of using nearest-neighbor extrapolation, one can also employ mirror extrapolation, where each background pixel is assigned the intensity of its mirrored counterpart across the anatomical boundary. This method aims to preserve local symmetry and can provide smoother boundary transitions in some cases.

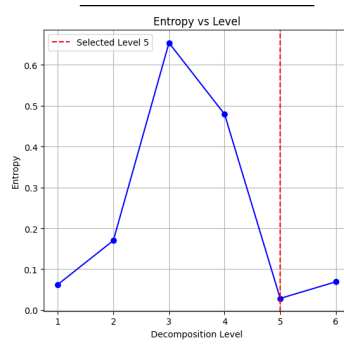


Figure 3.6: Entropy values plotted across different wavelet decomposition levels for the bias correction process. The red dashed line marks **Level 5**, which corresponds to the lowest entropy among all levels.

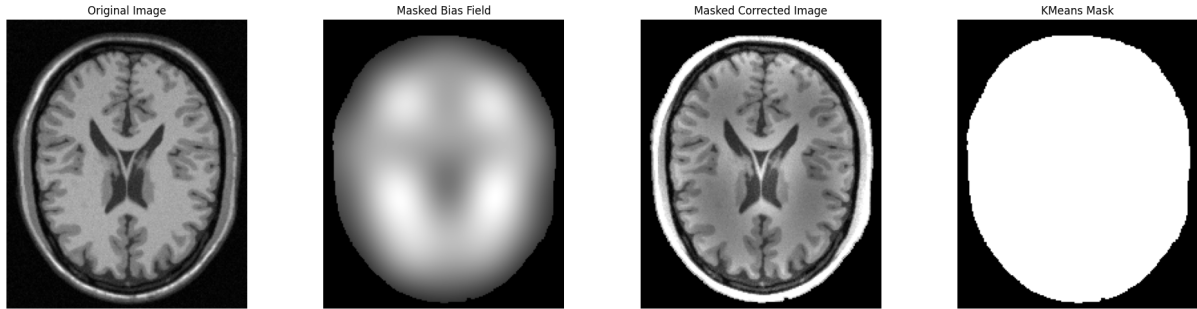


Figure 3.7: Illustration of the bias field correction process using KMeans masking. The first image shows the original MRI slice. The second image displays the estimated bias field over the brain region using the KMeans-generated tissue mask. The third image is the bias-corrected version of the input, showing improved tissue contrast and homogeneity. The fourth image presents the binary mask obtained via KMeans clustering, which identifies the brain region and excludes the background for focused correction. **This result corresponds to decomposition level 5 with the lowest entropy, indicating the most optimal bias correction.**

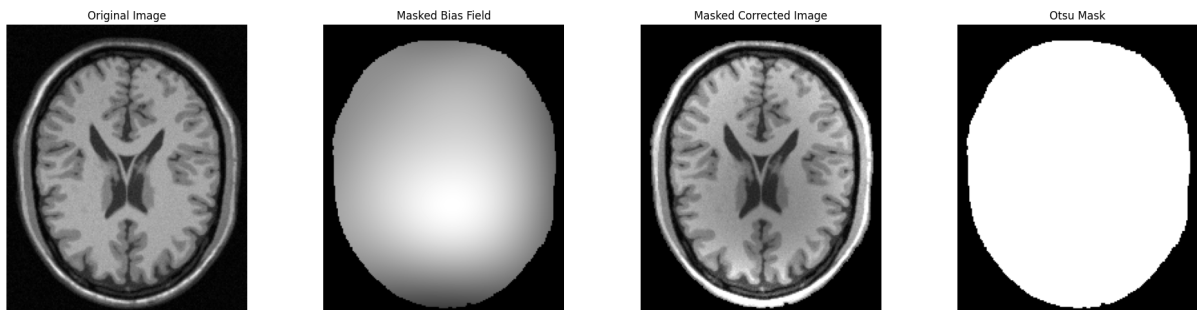


Figure 3.8: Bias field correction process using Otsu masking at **decomposition level 6 (non-optimal)**. The first panel displays the original MRI slice. The second panel shows the estimated bias field masked by the Otsu-based binary tissue mask. The third panel illustrates the bias-corrected image, demonstrating improved contrast but with suboptimal homogeneity compared to the best level. The fourth panel shows the Otsu-generated mask used for restricting the correction to brain regions. **This level was not selected as optimal based on the entropy criterion, which favored level 5 instead.**

4. Reconstruction Process

4.1. Aim

The aim of this section is to describe the MRI reconstruction pipeline developed during the internship, specifically focusing on the integration of bias field estimation with SENSE-like parallel imaging. The goal was to:

- Perform undersampled MRI acquisition simulation using synthetic coil sensitivity maps.
- Estimate smooth sensitivity maps using a wavelet-based Maximum-Value Projection (MVP) technique.
- Use these estimated maps to perform SENSE-like unaliasing reconstruction of undersampled coil data.
- Compare reconstructed results with ground truth and evaluate residual aliasing artifacts.

4.2. Methodology

4.2.1 Simulating Coil Sensitivity Profiles

Synthetic Gaussian-shaped sensitivity maps were generated for each coil, centered at different positions to mimic realistic surface coil behavior. Each coil's spatial sensitivity map $S_i(x, y)$ was defined as:

$$S_i(x, y) = \exp\left(-\frac{(x - x_i)^2 + (y - y_i)^2}{2\sigma^2}\right), \quad (4.1)$$

where (x_i, y_i) denotes the coil center and σ controls the spatial extent.

4.2.2 Simulating Undersampled Aliased Data

The full k-space data was simulated by applying a 2D Fourier transform to each coil image. Undersampling in the phase-encoding direction was then performed by removing lines in k-space based on a reduction factor R . This led to aliasing in the image domain.

4.2.3 Bias Field Estimation using MVP

The MVP algorithm was applied on each coil image to estimate the coil sensitivity maps of each coil. The process involved:

1. Performing multilevel wavelet decomposition using biorthogonal wavelets.
2. Suppressing high-frequency coefficients while retaining approximation coefficients.
3. Reconstructing the low-frequency image, which serves as the sensitivity map $B(x, y)$.

Each estimated map was normalized as:

$$\hat{S}_i(x, y) = \frac{B_i(x, y)}{\sqrt{\sum_{i=1}^N B_i^2(x, y)}} \quad (4.2)$$

to ensure RSS consistency across coils.

4.2.4 SENSE-like Reconstruction

The aliased image vector at each spatial location was modeled as:

$$\mathbf{y}(x, y) = \mathbf{S}(x, y) \cdot \boldsymbol{\rho}(x, y), \quad (4.3)$$

where $\mathbf{S}(x, y)$ is the coil sensitivity matrix and $\boldsymbol{\rho}(x, y)$ is the unaliased voxel vector.

The reconstruction was performed using the Moore–Penrose pseudoinverse:

$$\boldsymbol{\rho}(x, y) = (\mathbf{S}^H \mathbf{S})^{-1} \mathbf{S}^H \mathbf{y}(x, y). \quad (4.4)$$

To improve numerical stability, Tikhonov regularization was also tested:

$$\boldsymbol{\rho}_\lambda = (\mathbf{S}^H \mathbf{S} + \lambda \mathbf{I})^{-1} \mathbf{S}^H \mathbf{y}, \quad (4.5)$$

with λ as the regularization parameter.

4.3. Results and Observations

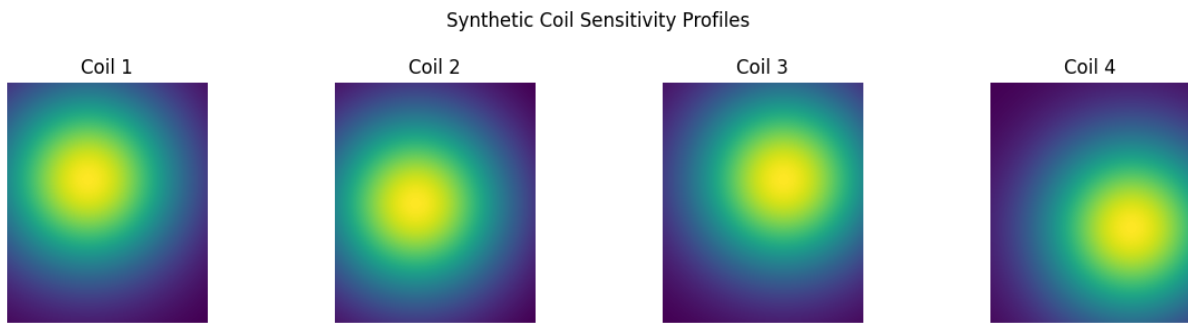


Figure 4.1: Synthetic surface coil sensitivity profiles for a 4-channel setup. Each map represents the spatially varying sensitivity of an individual surface coil modeled using Gaussian functions centered at different positions.

4.4. Bias Field Correction Results

In this section, we evaluate the effectiveness of an iterative wavelet-based Maximum Value Projection (MVP) with energy thresholding method for bias correction on individual coil images. Each coil’s spatial sensitivity introduces intensity inhomogeneities, which are corrected by estimating the low-frequency bias field using biorthogonal wavelet decomposition (bior4.4).

The optimal level is selected based on the inhomogeneity index of level, and bias correction is performed by dividing the original image by the estimated field. A Kmeans-generated brain mask localizes the correction to brain tissue, minimizing background influence.

4.4.1 Coil-wise Results

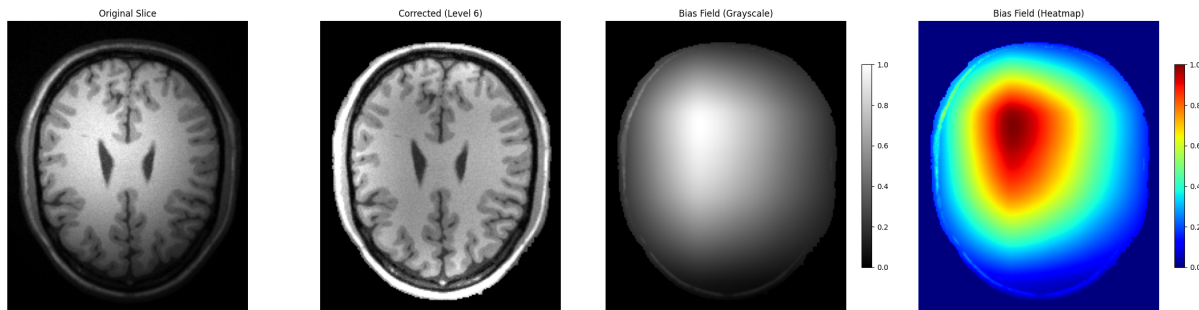


Figure 4.2: Bias field correction on Coil 1 image: (a) Original image, (b) Corrected image ($L = 6$), (c) Estimated bias field (grayscale), (d) Estimated bias field (heatmap).

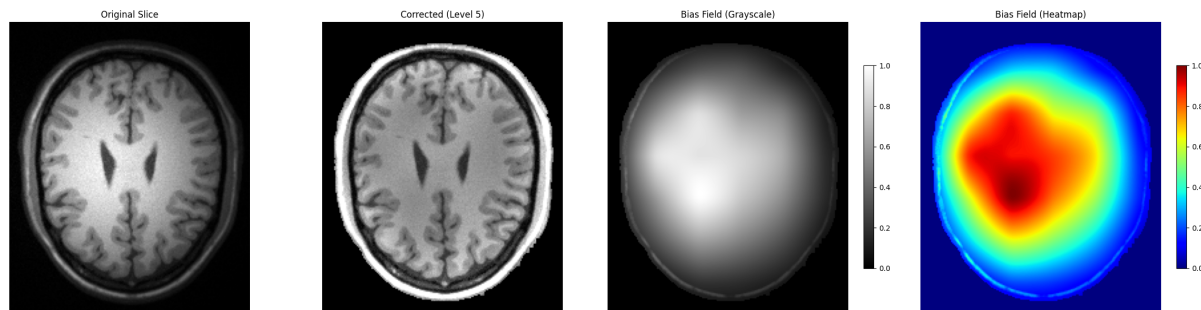


Figure 4.3: Bias field correction on Coil 2 image: (a) Original image, (b) Corrected image ($L = 5$), (c) Estimated bias field (grayscale), (d) Estimated bias field (heatmap).

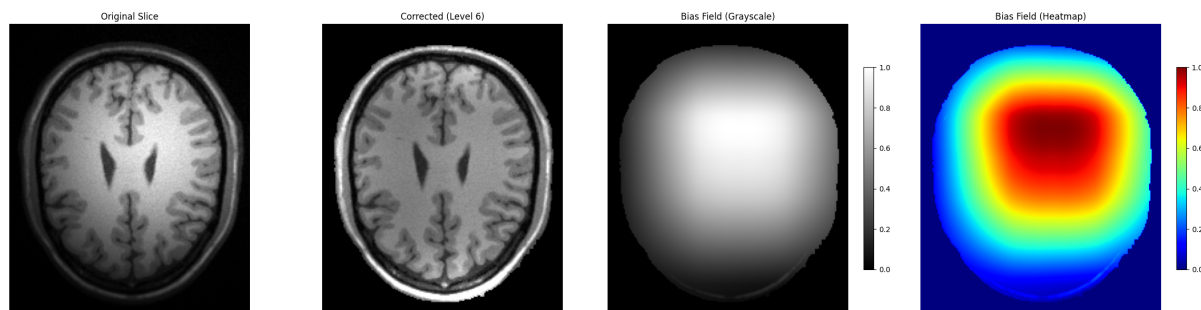


Figure 4.4: Bias field correction on Coil 3 image: (a) Original image, (b) Corrected image ($L = 6$), (c) Estimated bias field (grayscale), (d) Estimated bias field (heatmap).

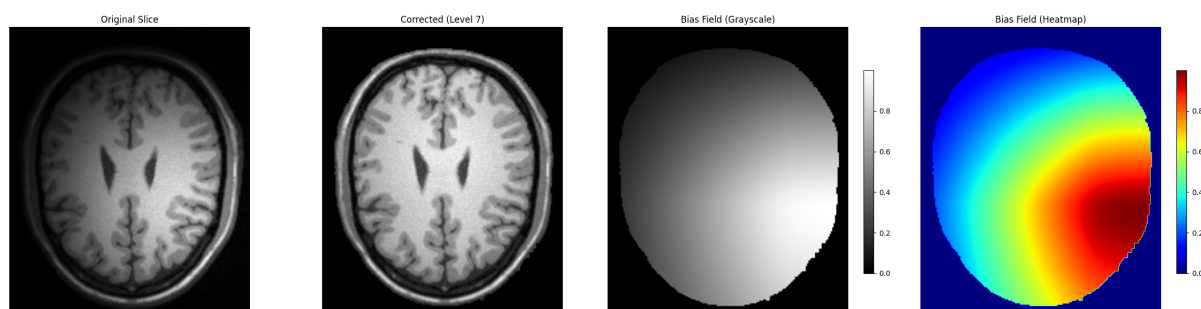


Figure 4.5: Bias field correction on Coil 4 image: (a) Original image, (b) Corrected image ($L = 7$), (c) Estimated bias field (grayscale), (d) Estimated bias field (heatmap).

4.4.2 Tikhonov-Regularized SENSE Reconstruction

SENSE reconstruction aims to recover full-FOV images from undersampled k-space using multiple coil sensitivities. The forward model is:

$$\mathbf{y} = \mathbf{S} \cdot \mathbf{x} + \mathbf{n}$$

where \mathbf{y} is the measured aliased data, \mathbf{S} the sensitivity matrix, \mathbf{x} the unaliased image, and \mathbf{n} noise.

A direct solution uses the pseudoinverse:

$$\hat{\mathbf{x}} = (\mathbf{S}^H \mathbf{S})^{-1} \mathbf{S}^H \mathbf{y}$$

But this is often unstable due to noise and ill-conditioning. To improve robustness, Tikhonov regularization adds a penalty term:

$$\hat{\mathbf{x}} = (\mathbf{S}^H \mathbf{S} + \lambda \mathbf{I})^{-1} \mathbf{S}^H \mathbf{y}$$

This stabilizes the inversion by balancing data fidelity and smoothness. The next figure compares results with and without regularization.

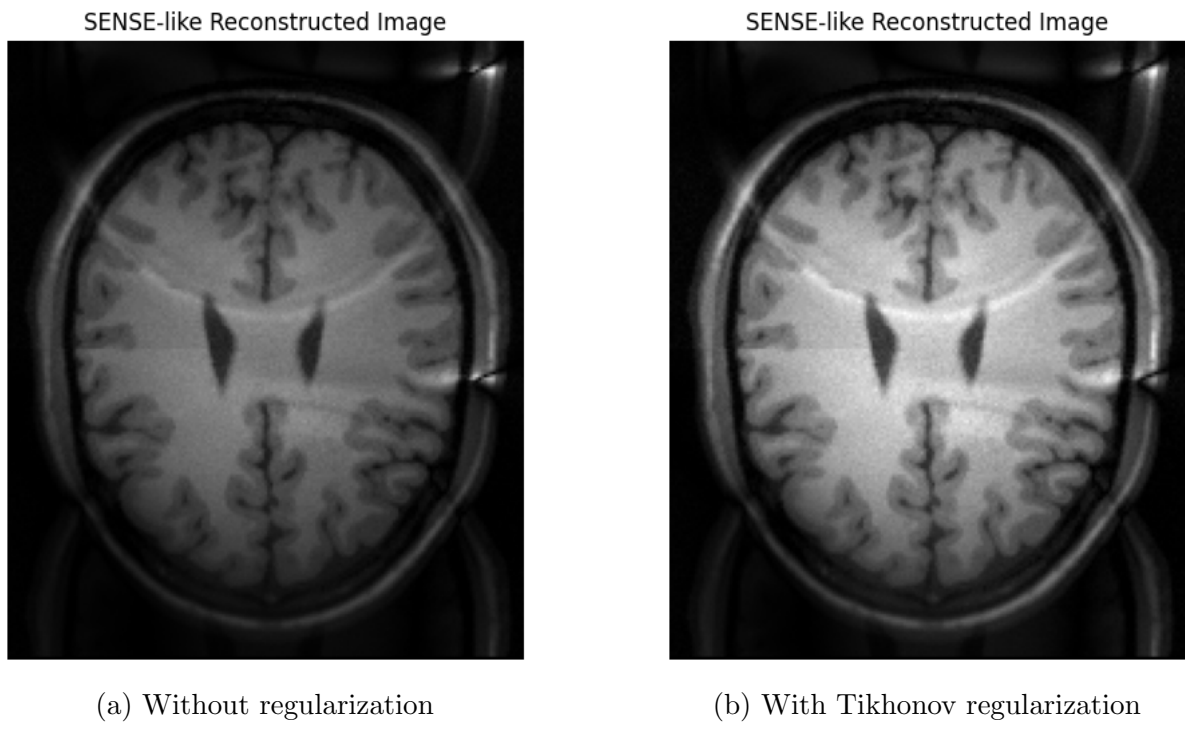


Figure 4.6: Comparison of SENSE-like reconstructed images. (a) Reconstruction using direct pseudo-inverse without any regularization, leading to contrast and aliasing artifacts. (b) Reconstruction using Tikhonov-regularized inversion, resulting in reduced artifacts and improved robustness. Aliasing artifacts can be mitigated through accurate sensitivity calibration.

5. Conclusion and Future Work

5.1. Conclusion

This work successfully implemented a wavelet-based Maximum Value Projection (MVP) method, including enhancements such as energy-based thresholding and nearest-neighbor extrapolation, for surface coil bias correction. These techniques were integrated into a SENSE-like reconstruction pipeline. The MVP method effectively estimated smooth low-frequency bias fields, improving intensity uniformity across individual coil images. When incorporated into the SENSE reconstruction, the estimated sensitivity maps produced clearer, artifact-reduced images, particularly when combined with Tikhonov regularization.

5.2. Future Work

Future efforts could focus on extending this method to 3D volumetric datasets and evaluating performance on real multi-channel MRI acquisitions. Incorporating advanced machine learning techniques for sensitivity map estimation and bias modeling may further enhance robustness and reconstruction quality.

References

1. B. Belaroussi, J. Milles, S. Carme, Y. M. Zhu, and H. Benoit-Cattin, "Intensity non-uniformity correction in MRI: Existing methods and their validation," *Medical Image Analysis*, vol. 10, no. 2, pp. 234–246, 2006. doi:10.1016/j.media.2005.09.004.
2. F.-H. Lin, Y.-J. Chen, J. W. Belliveau, and L. L. Wald, "A wavelet-based approximation of surface coil sensitivity profiles for correction of image intensity inhomogeneity and parallel imaging reconstruction," *Human Brain Mapping*, vol. 19, no. 2, pp. 96–111, 2003. doi:10.1002/hbm.10109.
3. S. Shen, W. A. Sandham, M. H. Granat, and A. Sterr, "Intensity non-uniformity correction of magnetic resonance images using a fuzzy segmentation algorithm," in *Proceedings of the 27th Annual International Conference of the IEEE Engineering in Medicine and Biology Society (EMBS)*, Shanghai, China, Sep. 2005, pp. 3035–3037. doi:10.1109/IEMBS.2005.1617057.
4. H. Cheng, F. Huang, Q. Zhao, and M. Limkeman, "Intensity correction using image extrapolation and multi-resolution analysis," in *Proceedings of the International Society for Magnetic Resonance in Medicine (ISMRM)*, vol. 13, Miami, FL, USA, 2005, p. 2755.
5. J. Karam and S. E. Mansour, "On the roots of Daubechies polynomials for biorthogonal wavelets," in *Proceedings of the 2012 International Conference on Communications and Information Technology (ICCIT)*, Hammamet, Tunisia, 2012, pp. 394–396. doi:10.1109/ICCI Technol.2012.6285823.
6. X. J. Zhou, M. A. Bernstein, and K. F. King, *Handbook of MRI Pulse Sequences*. Elsevier Academic Press, 2004. ISBN: 978-0-12-092861-3.
7. P. P. Vaidyanathan, *Multirate Systems and Filter Banks*. Pearson Education, 2006. ISBN: 8177589423.
8. R. W. Brown, Y.-C. N. Cheng, E. M. Haacke, M. R. Thompson, and R. Venkatesan, *Magnetic Resonance Imaging: Physical Principles and Sequence Design*. Elsevier Academic Press, 2004. ISBN: 978-0-12-092861-3.